Slow Inactivation in *Shaker* K Channels Is Delayed by Intracellular Tetraethylammonium

Vivian González-Pérez,[1,2] Alan Neely,[1] Christian Tapia,[1,2] Giovanni González-Gutiérrez,[1,2] Gustavo Contreras,[3] Patricio Orio,[1] Verónica Lagos,[1] Guillermo Rojas,[1,2] Tania Estévez,[1] Katherine Stack,[1] and David Naranjo[1]

[1]Centro de Neurociencias de Valparaíso and Departamento de Neurociencias, [2]Programa de Doctorado en Ciencias, mención Neurociencia, and [3]Programa de Magister en Ciencias, mención Neurociencia, Universidad de Valparaíso, 2349400 Valparaíso, Chile

After removal of the fast N-type inactivation gate, voltage-sensitive *Shaker* (*Shaker* IR) K channels are still able to inactivate, albeit slowly, upon sustained depolarization. The classical mechanism proposed for the slow inactivation observed in cell-free membrane patches—the so called C inactivation—is a constriction of the external mouth of the channel pore that prevents K^+ ion conduction. This constriction is antagonized by the external application of the pore blocker tetraethylammonium (TEA). In contrast to C inactivation, here we show that, when recorded in whole *Xenopus* oocytes, slow inactivation kinetics in *Shaker* IR K channels is poorly dependent on external TEA but severely delayed by internal TEA. Based on the antagonism with internally or externally added TEA, we used a two-pulse protocol to show that half of the channels inactivate by way of a gate sensitive to internal TEA. Such gate had a recovery time course in the tens of milliseconds range when the interpulse voltage was −90 mV, whereas C-inactivated channels took several seconds to recover. Internal TEA also reduced gating charge conversion associated to slow inactivation, suggesting that the closing of the internal TEA-sensitive inactivation gate could be associated with a significant amount of charge exchange of this type. We interpreted our data assuming that binding of internal TEA antagonized with U-type inactivation (Klemic, K.G., G.E. Kirsch, and S.W. Jones. 2001. *Biophys. J.* 81:814–826). Our results are consistent with a direct steric interference of internal TEA with an internally located slow inactivation gate as a "foot in the door" mechanism, implying a significant functional overlap between the gate of the internal TEA-sensitive slow inactivation and the primary activation gate. But, because U-type inactivation is reduced by channel opening, trapping the channel in the open conformation by TEA would also yield to an allosteric delay of slow inactivation. These results provide a framework to explain why constitutively C-inactivated channels exhibit gating charge conversion, and why mutations at the internal exit of the pore, such as those associated to episodic ataxia type I in hKv1.1, cause severe changes in inactivation kinetics.

INTRODUCTION

In neuronal cells, sustained or prolonged depolarization inactivates voltage-gated potassium channels, favoring an increase in excitability. Slow inactivation was first described as a reduction in potassium permeability in the squid-delayed rectifier after holding the giant axon at voltages around 0 mV (Ehrenstein and Gilbert, 1966). It was not until the beginning of the nineties that works on voltage-gated *Shaker* K channels from the laboratories of Aldrich and Yellen set the groundwork for what is now the classical view of potassium channel slow inactivation. They described two types of inactivation processes, the N-type and the C-type inactivation, each having different molecular bases. The N-type inactivation occurs when a movable protein segment localized toward the N terminus of the protein blocks ion conduction by binding to the open conformation of the internal entrance of the pore (Hoshi et al., 1990; Zagotta et al., 1990; Demo and Yellen, 1991). Removal of part of the N terminus of *Shaker* abolishes N inactivation but uncovers another, slower inactivation process reminiscent of the one observed in the squid axon, the so-called C inactivation (Hoshi et al., 1990). Structural determinants of the C inactivation appear to be localized toward the external entrance of the pore (see Fig. 1 in Oliva et al., 2005) and toward the N terminus of the sixth transmembrane segment of the protein (Hoshi et al., 1991). In the conventional view, the C-inactivated state is produced by a localized constriction of the external mouth of the channel, which thereby interrupts K^+ ion conduction. Such conformational change is antagonized by the extracellular addition of K^+ ions (López-Barneo et al., 1993; Baukrowitz and Yellen, 1996;

Correspondence to David Naranjo: david.naranjo@uv.cl

Abbreviations used in this paper: COVC, cut-open oocyte voltage clamp; MES, methanesulfonic acid; NMG, *N*-methyl-D-glucamine; TEVC, two-electrode voltage clamp.

The Rockefeller University Press $30.00
J. Gen. Physiol. Vol. 132 No. 6 633–650
www.jgp.org/cgi/doi/10.1085/jgp.200810057

Molina et al., 1998) or TEA, a generalist K channel blocker (Choi et al., 1991; Yellen, 1998).

Today, other slow inactivation processes have been described for *Shaker* K channels, involving additional components of the protein (Olcese et al., 1997; Loots and Isacoff, 1998; Klemic et al., 2001). The voltage sensor gets engaged in a highly stable set of conformational states, even in constitutively slow inactivated channels (Olcese et al., 1997). Moreover, mutations at the internal mouth of the pore severely alter the slow inactivation rate, suggesting an involvement of this structure in slow inactivation (Holmgren et al., 1997; D'Adamo et al., 1998; Klement et al., 2008). In other voltage-gated K channel subfamilies, a functional correlation between the intracellular entrance and slow inactivation has been found. For example, during slow inactivation gating, Kv1.4 extrudes a volume of water toward the cytosolic side of the channel that is comparable to that displaced during activation (Jiang et al., 2003). Also, slow inactivation in Kv2.1 is interfered by internal TEA (Kerschensteiner et al., 2003).

Here, we show that in whole cell recordings from *Xenopus* oocytes expressing N inactivation–removed *Shaker* K channels, at least half of the channels inactivate by a mechanism that is interfered by internal TEA. Such TEA sensitivity, similar to that of the activation gate, is in contrast to conventional C inactivation mechanism. Internal TEA also prevents a significant amount of gating charge conversion associated to slow inactivation by Olcese et al. (1997), suggesting that part of this charge exchange is not functionally associated with C-type inactivation. These data are consistent with a closed state–accessed inactivation as a U-type inactivation mechanism (Klemic et al., 2001), in which an open channel blocker causes an allosteric delay of slow inactivation by trapping the channels in the open conformation. But, the inactivation delay produced by internal TEA is also consistent with the existence of an internally located slow inactivation gate, sterically interfered by this quaternary ammonium. Such type of gates have been proposed before for HCN and Kv4.2 channels (Shin et al., 2004; Dougherty et al., 2008), and for the ultraslow inactivation in Na channels (Sandtner et al., 2004), suggesting a common repertoire of nonconducting conformations for members of the voltage-gated ion channel family.

MATERIALS AND METHODS

Salts were purchased from Merck Chile S.A, and gentamicin, EGTA, HEPES, and methanesulfonic acid (MES) were from Sigma-Aldrich. Agitoxin II was purchased from Alomone Laboratories, and type 2 collagenase was from Worthington Biochemical Corporation.

Heterologous Expression of Shaker K Channels

Our background construct was derived from a *Shaker* H4 Δ(6–46), here called *Shaker* IR, inserted in pBluescript SK vector under the command of the T7 promoter (Agilent Technologies). Point mutations were performed by PCR using two mutation–containing complementary synthetic oligonucleotides extended by *Pfu* polymerase over the *Shaker* template (QuickChange; Agilent Technologies). The PCR product was digested with AccI and BamHI, and the 388-bp fragment (Goldstein et al., 1994) was subcloned back into the plasmid carrying *Shaker*. Constructs were verified by automated sequencing of the AccI-BamHI cassette after subcloning (Macrogen). Capped cRNAs for *Shaker* IR and mutants were synthesized from a NotI-linearized template using MESSAGE machine (Applied Biosystems), resuspended in 10 µl water, and stored at −80°C until use.

Female *Xenopus laevis* frogs were purchased from local providers who captured them in the vicinity of Valparaíso. They were kept in captivity for several months, in accordance with the Guide for the Care and Use of Laboratory Animals (1996, National Academy of Sciences, Washington, DC), at 18°C, with a constant 24-h light-dark cycle. To remove oocytes, the frogs were anesthetized with 0.5% ethyl 3-amino-benzoato MES salt. Follicular membranes were separated by 1–2-h treatment with 3 mg/ml collagenase type 2 at room temperature. After several washes, the oocytes were kept at 18°C in a solution (SOS) containing (in mM): 96 NaCl, 2 KCl, 1.8 $CaCl_2$, 1 $MgCl_2$, 5 HEPES, pH 7.4. 0.1–1 ng cRNA was injected in a volume of 50 nl using a nanoject 2000 injector (WPI). During injection, oocytes were kept in a similar solution to SOS, with all Ca^{2+} being replaced with extra Mg^{2+}. Oocytes were incubated at 18°C in SOS solution supplemented with 2.5 mM sodium pyruvate and 100 µg/ml gentamycin sulfate until recording.

Electrophysiological Recordings

For experiments with external perfusion of TEA, two-electrode voltage clamp (TEVC) was performed with either an OC-725 (Warner Instruments) or a TEV-200 amplifier (Dagan Corporation). Voltage pulses and data acquisition were obtained through a PCI-MIO-16XE-10 card (National Instruments Corp.) under the control of the WinWCP software (University of Strathclyde, Glasgow, Scotland). TEVC traces were usually filtered to 1 kHz with the output filter of the amplifier and digitized at 0.25–10 kHz. The voltage and current electrode were filled with a solution of 3 M KCl, 1 mM EGTA, and 5 mM HEPES-KOH, pH 7.0, and had resistances of 0.3–1.0 MΩ. TEVC recording solution was composed of (in mM): 96 NaCl, 2 KCl, 1 $MgCl_2$, 0.2 $CaCl_2$, and HEPES-NaOH, pH 7.4. Usually, TEA was added to this solution by equivalent replacement of Na to keep ionic strength constant, except for the experiments shown in Figs. 3 and 4, in which TEA or *N*-methyl-D-glucamine (NMG) were added to the solution without compensating for ionic strength. For the long measurements of voltage-dependent slow inactivation at near steady state (Figs. 2 and 4), channel availability was tested after 60-s long voltage prepulse by a 5-s pulse to 50 mV (60-s isochronal inactivation). To minimize electrode polarization produced by these long voltage pulses, the amount of cRNA injected was adjusted to keep the ionic current size at <4 µA. In addition, the voltage electrode potentials were measured at the end of each experiment (see details in Oliva et al., 2005), and experiments having voltage drift of >±5 mV were rejected.

For experiments with internal perfusion of TEA, cut-open oocyte voltage clamp (COVC) experiments were made with a Dagan CA-1B amplifier (Taglialatela et al., 1992). Voltage pulses and data acquisition were performed through a Digidata 1200 card (MDS Analytical Technologies) under the command of the pClamp 8 software suite (MDS Analytical Technologies). To gain perfusional and electrical access to the intracellular side, the bottom of the oocyte was permeabilized by a brief treatment with 0.1% saponin. Pipettes were filled with 2 M tetramethylammonium-MES, 50 mM NaCl, and

10 mM EGTA and yield resistance from 0.5 to 1.2 MΩ. For the recording of ionic currents, the external solution was usually composed of (in mM): 100 NaCl, 25 KCl, 2 $MgCl_2$, 1.8 $CaCl_2$, and 5 HEPES, pH 7.2. The internal solution contained 120 KMES, 0.1 EGTA, and 10 HEPES, pH 7.0. For the gating current measurements, the external solutions was (in mM) 120 NMG, 2 $CaCl_2$, and 10 HEPES titrated with MES acid, pH 7.0, plus 5 μM agitoxin II, whereas the internal solution was 120 NMG, 0.1 EGTA, and 10 HEPES titrated with MES acid, pH 7.0. In earlier experiments with 10 or 1 mM EGTA in the internal solution, we consistently observed rundown of the K currents, usually without detectable effects on gating. We avoided this inconvenience by lowering EGTA concentration to 0.1 mM. To ensure the stability of the current sizes, we monitored the K channel activity for at least 20 min before the beginning of internal perfusion of TEA.

The COVC is a low-impedance voltage-clamp technique with several sources of leakage currents needing to be electronically compensated. These currents are completely eliminated with the usual linear capacitance and leakage digital subtraction protocols as described for the giant squid-axon voltage clamp (Taglialatela et al., 1992). This subtraction is not feasible with pulses lasting tens of seconds and recoveries in the time scale of the pulse protocol. Thus, uncertainties about true zero current level remain within ±100 nA, and currents leaking between the recording and the guard pools as large as the latter figure may be added to the uncorrected K current. This artifact contaminates all data obtained with COVC.

Signal analyses and curve fitting were done with Clampfit 9 (MDS Analytical Technologies) and Microcal Origin 3.5 and 4.1 (Microcal). With both electrophysiological techniques, two exponential functions were usually required to fit the time course of inactivation; however, to simplify the analysis, all relaxations were fit to single exponentials. We found a day-to-day variability in the inactivation time constant that could be attributed to uncontrolled changes in room temperature of up to 5°C or to variability in the extent of C-type inactivation in whole oocyte due to individual *X. laevis* variability.

Current Simulations

Simulations of an allosteric model of *Shaker* K channel with an activation and two inactivation pathways (Klemic et al. 2001) were conduced within the NEURON simulation environment (Hines and Carnevale, 1997; http://www.neuron.yale.edu). The P/C inactivation pathway was called C instead of I_P for the classical C inactivation, and I_U was called U. The model was used with the published values for the rate constants and allosteric factors. The model had three additional states that were blocked with TEA applied internally: an open-blocked, a C-inactivated–blocked, and a U-inactivated–blocked state (Fig. 13). All bind TEA in a voltage-independent fashion with association and dissociation rate constants of 2.4 $ms^{-1}mM^{-1}$ and 2.4 ms^{-1}, respectively. The channels were modeled in the surface of a cylindrical compartment having only a K-selective conductance with a maximal value of g_{max} = 3.5 mS/cm^2. External and internal potassium ion concentrations were set to 25 and 140 mM, respectively. Ionic currents were calculated with the expression $I = g_{max}P_o(Vm\text{-}E_K)$, where P_o, Vm, and E_K are the channel open probability, the membrane potential, and the Nernst potential for K^+, respectively. The gating currents, I_g, were calculated according to Bezanilla (2000): $I_g = \Sigma_{i,j} I_{ij}$, where I_{ij} is gating current contributed by each voltage-dependent transition between states S_i and S_j according to: $I_{ij} = z_{ij}(\mathbf{S}_i k_{Vij} - \mathbf{S}_j k_{-Vji})$, with z_{ij} being the net charge displaced, k_{Vij} and k_{-Vji} being the forward and backward rates, and $\mathbf{S}_i$ and $\mathbf{S}_j$ being the probabilities of states S_i and S_j.

RESULTS

Sensitivity of Slow Inactivated Shaker to External TEA

In response to a voltage step pulse to 0 mV, *Shaker* K channels lacking N-type inactivation (*Shaker* IR) rapidly activate and then slowly inactivate so that at the end of a 15-s pulse their activity is reduced to ∼25% of their peak value (see for example Olcese et al., 1997; Yang et al., 1997; Klemic et al., 2001; Oliva et al., 2005). In the classical C inactivation paradigm (Choi et al., 1991), the decay in current represents mostly channels going from the open conformation to the inactivated state. This inactivated state is produced by a localized constriction of the external mouth of the channel, which interrupts K^+ ion conduction (Yellen et al., 1994; Liu et al., 1996). Such conformational change is sterically prevented when TEA, a generalist potassium channel blocker, binds to the external entrance of the pore in a mutually exclusive fashion. Consistent with such a functional picture of inactivation, we can draw the following scheme (Choi et al., 1991):

$$B_{ex} \overset{K_{Dex}}{\longleftrightarrow} O \underset{k_r}{\overset{k_i}{\rightleftharpoons}} I$$

SCHEME 1

where I, O, and B_{ex} correspond to the inactivated, the open-unblocked, and the TEA-blocked channels, respectively. The blockade by TEA equilibrates rapidly with a dissociation constant K_{Dex}, whereas inactivation and recovery are first-order processes having rate constants k_i and k_r, respectively. Scheme 1 indicates that slow inactivation can only occur from open-unblocked channels; thus, as the external TEA concentration is increased, the effective inactivation rate is reduced according to k_i times the unblocked fraction. On the other hand, the recovery rate is independent of external TEA provided that the inactivated state does not bind TEA. Thus, only the onset of the slow inactivation kinetics should be delayed by TEA. Contrary to these expectations, Fig. 1 shows that with TEVC, the effect of external TEA on the time course of inactivation was very modest, even at concentrations blocking 80% of the K currents.

Fig. 1 A shows current traces in the presence of increasing concentrations of TEA at constant ionic strength. A first observation was that, as expected, TEA inhibited *Shaker* K channels, producing a reduction in the size of the currents. The inset in Fig. 1 summarizes results from several oocytes where the fractional unblocked peak current is plotted against the external TEA concentration. The continuous line is a single-site inhibition isotherm with a K_{Dex} of 18 mM.

Despite knowing that slow inactivation arises from complex multistate processes (see for example Olcese

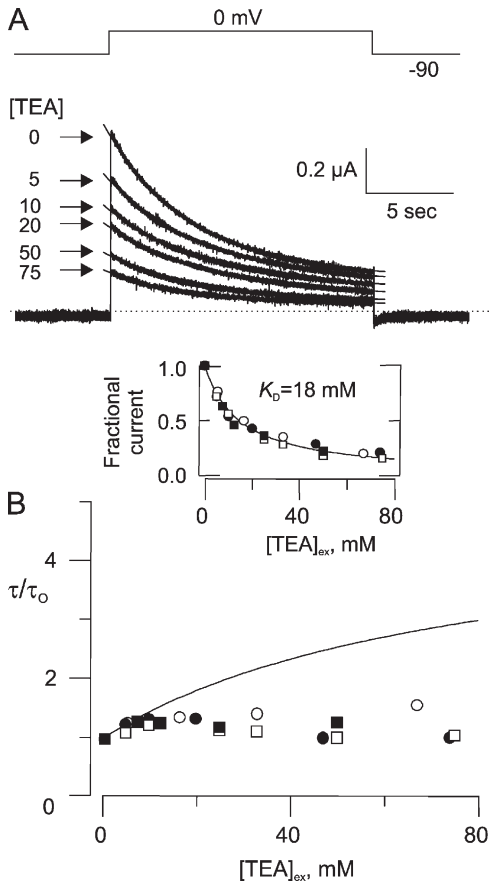

Figure 1. Slow inactivation in *Shaker* IR is weakly sensitive to external TEA. (A) The ionic current traces were elicited by a 15-s pulse to 0 mV protocol schematized at the top of the figure. The TEA concentrations, listed near each trace, were obtained by equivalent replacement of NaCl by TEACl to keep ionic strength constant in the bath solution. The continuous lines on top of each trace are the fits to a single exponential function with time constants of: 4.9, 5.5, 5.8, 5.8, 4.9, and 4.5 s for the traces indicated with [TEA] = 0, 5, 10, 20, 50, and 75 mM, respectively. The dashed line indicates the zero current level. (Inset) Unblocked fractional peak current as a function of the external TEA. Each family of symbol corresponds to a different oocyte. The continuous line was drawn according to an inhibition isotherm with a K_D of 18 mM for TEA. (B) Normalized time constant as a function of the external TEA concentration. Each family of symbols corresponds to the same oocytes as in the inset. The continuous line was draw according to the prediction of Scheme 1, with $\tau/\tau_0 = (k_i \times U + k_r)^{-1}$, where τ/τ_0 is the fold increase in time constant, U the fractional unblocked current in the presence of TEA, and k_i and k_r are equal to 0.19 s^{-1} and 0.05 s^{-1}, respectively (Oliva et al., 2005). In average for *Shaker* IR, τ_0 = 4.5 ± 0.9 s (n = 12).

et al., 1997; Loots and Isacoff, 1998; Klemic et al., 2001; Oliva et al., 2005), we evaluated the effect of TEA on inactivation kinetics by fitting mono-exponential functions to the current decays (continuous lines on top of the traces in Fig. 1 A). Typical decay time constants measured at 0 mV were ~5 s in the absence TEA (see Oliva et al., 2005). The resulting normalized time constants at different TEA concentrations are plotted in Fig. 1 B for several oocytes. Below 15 mM, and consistent with Scheme 1, external TEA induces a modest, although significant, increase in the inactivation time constant. For example: *tau* values for [TEA] between 15 and 20 mM are 30% larger than in the absence of TEA (one-tail t test, P = 0.005; five oocytes). However, at blocker concentrations >20 mM, and in agreement with Yang et al. (1997), the inactivation kinetics departed drastically from the expected behavior predicted by the antagonism between TEA and slow inactivation (continuous line in Fig. 1 B).

We tested if TEA affected the voltage dependence of near steady-state inactivation by measuring the current elicited after a 1-min-long conditioning prepulse (60-s isochronal inactivation; see Materials and methods). To optimize our ability to detect changes in the apparent voltage dependence without drastically compromising the size of the currents, we used a TEA concentration two- to threefold over the K_{Dex} (Figs. 2 and 4). Fig. 2 shows recordings of ionic current obtained in the absence of TEA (A) and in the presence of 40 mM TEA maintaining ionic strength constant (B). With the proviso that K currents clearly had not reached equilibrium at the end of the 60 s (see control traces in Fig. 2 A), the current amplitude measured at 200 ms in response to the +50 mV test pulse is plotted as a function of the conditioning pulse voltage in Fig. 2 C before (open circles) and after the addition of TEA (filled circles). Voltage dependence of these isochronal inactivation data was fitted to a single Boltzmann distribution function to compare the apparent energetic impact of external TEA on slow inactivation. For eight oocytes for which the full voltage excursion was obtained with and without 40 mM TEA, $V_{0.5}$ was −34.5 ± 1.0 and −35.2 ± 1.3 mV, respectively These $V_{0.5}$ values were not significantly different (P = 0.685; unpaired two-tailed t test). The inset in Fig. 2 C shows the relationships of the conductance at steady state versus voltage, taken before and after the measurements, to monitor drifts in the voltage-sensing electrode potential during these measurements. Together with results shown in Fig. 1, we conclude that slow inactivation in whole oocytes is weakly sensitive to the presence of external TEA and is therefore clearly inconsistent with the classical description for C inactivation.

Shaker IR T449S is a variant that slow inactivates with the classical external pore-collapse mechanism (C inactivation; López-Barneo et al., 1993; Jerng and Gilly, 2002), so we tested the effect of external TEA on this mutant. Fig. 3 A shows current traces of *Shaker* T449S elicited by a 5-s pulse to 0 mV, recorded in the presence of increasing external TEA concentrations. In this variant, macroscopic inactivation is ~10-fold faster than in *Shaker* IR, and the apparent affinity for TEA is increased by about fivefold, with a K_{Dex} = 4.2 ± 0.2 mM (n = 4; Fig. 3, inset). As before, we fitted a single exponential function to the current decays (lines on top of the traces)

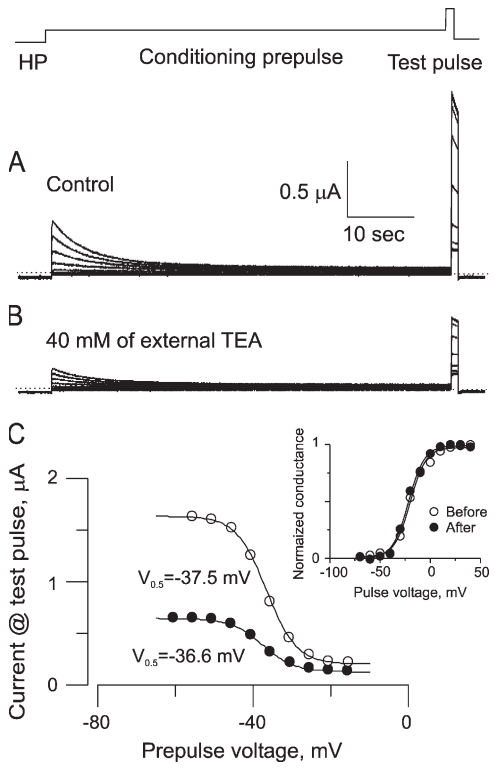

Figure 2. Voltage dependence of *Shaker* IR channel availability in the presence of external TEA. (A) Ionic currents in the absence of TEA elicited after the protocol schematized at the top of the figure. This protocol consisted of a 60-s prepulse to voltages usually ranging from −70 to −15 mV with 5-mV steps. At the end of this period, channel availability was tested with a pulse to +50 mV. (B) Similar traces in the presence of 40 mM TEACl replacing an equivalent concentration of NaCl. (C) Comparison of the peak current amplitude at the test voltage pulse for the control traces shown in A (open circles) and the 40-mM external TEA traces in B (filled circles). The continuous lines are fits to a Boltzman distribution function with the half inactivation voltages depicted in the figure and an effective valence of $z = -6.34\ e_o$ for the control traces and $z = -6.63\ e_o$ for the TEA traces. HP, the holding voltage was −90 mV. Discontinuous lines in A and B indicate zero current level. (Inset) Activation relationship measured at the end of a 50-ms pulse taken before (open circles) and after (filled circles) the inactivation protocols for the experiments shown. Conductances were calculated assuming a reversal potential of −100 mV. Continuous lines are a Boltzman distribution equation with $V_{0.5}$ = −20.0 and −21.7 mV for the before and after data, respectively, with effective valences of 3.2 and 3.3, respectively.

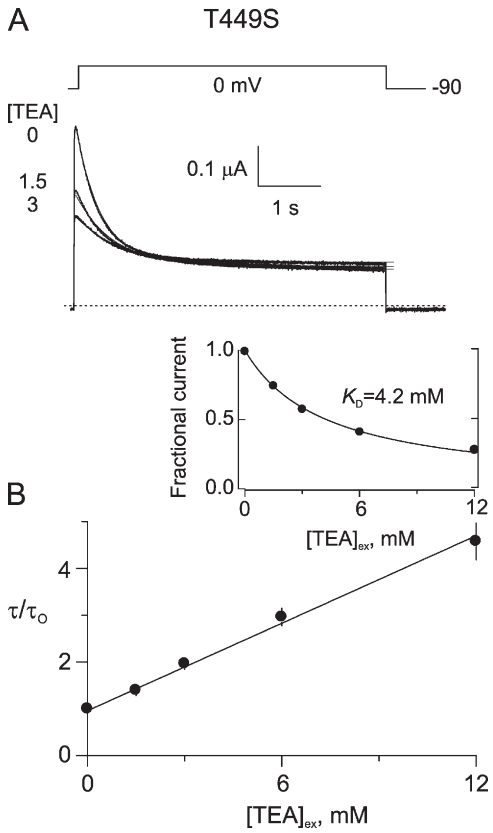

Figure 3. Inactivation kinetics in *Shaker* IR T449S is slowed down by external TEA. (A) Ionic current traces elicited by a 5-s pulse to 0 mV as depicted on the top of the figure. Shown are traces in 0, 1.5, and 3 mM of external TEA added to the recording solution. Continuous lines at the top of the traces are fits to a single exponential function with time constants of 0.38, 0.60, and 0.84 s, for 0, 1.5, and 3 mM TEA, respectively. For longer pulses a slower component becomes evident. (Inset) Unblocked fractional peak current as a function of the external TEA. Each data point corresponds to the average of at least three oocytes. In some instances the error bars are smaller than the symbol size. The continuous line was draw according to an inhibition isotherm with a K_D of 4.2 mM for TEA. (B) Normalized time constant as a function of the external TEA concentration. The continuous line is the fit of a linear regression with slope = 0.31 fold/mM, consistent with a K_D = 3.2 mM according to Scheme 1. $\tau_0 = 0.35 \pm 0.2$ ($n = 6$).

and plotted the effect of TEA on the time constants Fig. 3 B. It is clear that in this mutant, external TEA delays slow inactivation kinetics. The time constant increased linearly with TEA in a manner consistent with Scheme 1 (assuming a small recovery rate). Fig. 4 shows that the voltage dependency of near steady-state inactivation was significantly shifted toward positive voltages in the presence of 12 mM of external TEA added on top of the recording solution (Fig. 4 B). The single Boltzmann distribution fit to the voltage dependency of near steady-state inactivation for this *Shaker* variant gave $V_{0.5}$ values of −44.0 ± 0.5 mV ($n = 11$) and −38.4 ± 1.5 mV ($n = 5$) for the control and 12 mM TEA, respectively (P = 0.0002; two-tailed unpaired *t* test). This +5.5 mV shift appears to be specific for the presence of TEA in the external solution and is not due to the increase in ionic strength because the addition of 12 mM NMG-MES to the bath produced a shift of only +1.5 ± 0.8 mV ($n = 5$). Although we cannot discard additional effects produced by the binding of external TEA to the closed channels, these results together with those shown in Fig. 3 indicate that, unlike *Shaker* IR, both the kinetics of inactivation and near steady-state inactivation are sensitive to the presence of external TEA in *Shaker*–IR-T449S, consistent with the conventional C inactivation mechanism.

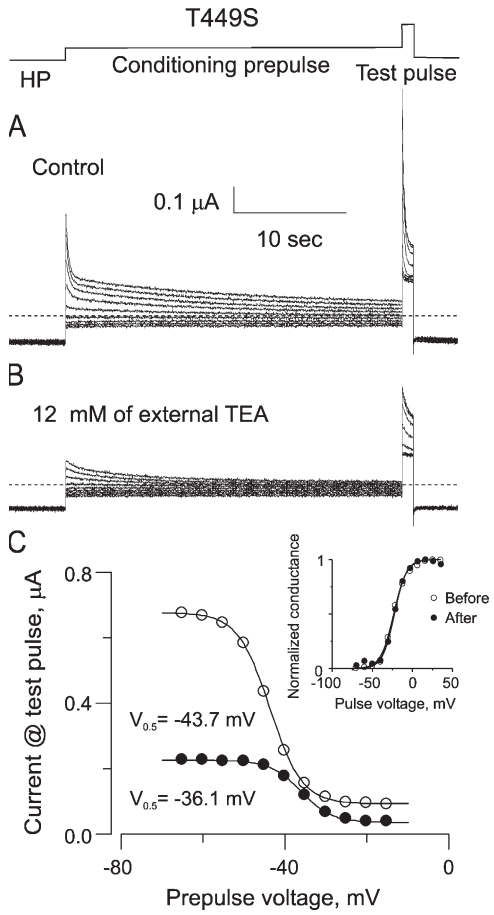

Figure 4. Voltage dependence of *Shaker* IR T449S channel availability in the presence of external TEA. (A) Ionic currents in the absence of TEA elicited after the protocol schematized at the top of the figure. This protocol is similar to that shown in Fig. 2, except that the voltage pre-pulses were 30 s long. Inactivation kinetics clearly show two components, with time constants at ~0.3 and ~15 s. (B) Similar traces in the presence of 12 mM TEACl added to the recording solution. Consistent with data shown in Fig. 3, TEA not only blocks the current, but also drastically changes its kinetic. (C) Comparison of the peak current amplitude at the test voltage pulse for the control traces shown in A (open circles) and with 12 mM of external TEA in B (filled circles). The continuous lines are fits to a Boltzman distribution function with the half inactivation voltages depicted in the figure using an effective valence of $z = -6.56\ e_o$ for the control traces and $z = -6.92\ e_o$ for the TEA traces. Discontinuous lines in A and B indicate zero current level. (Inset) Activation relationship measured 10 ms into the activation voltage pulse taken before (open circles) and after (filled circles) the inactivation protocols for the experiments shown. Conductances were calculated assuming a reversal potential of −100 mV. Continuous lines are a Boltzman distribution equation with $V_{0.5}$ = −23.4 and −22.5 mV for the before and after data, respectively, with effective valences of 3.2 and 3.4, respectively.

A Slow Inactivation Sensitive to Internal TEA

At present, there are some hints that in some voltage-gated K channels an inactivation gate, or part of it, is localized toward the cytosolic entrance of the pore. For example, internal TEA delays slow inactivation in Kv2.1 channels (Kerschensteiner et al., 2003). On the other hand, the osmotic work performed by the Kv1.4 *Shaker* homologue during gating revealed equivalent volumetric changes in the internal vestibule during slow inactivation, activation, and deactivation (Jiang et al., 2003). Thus, the conformational changes that occur during activation and slow inactivation gates could be structurally similar and share functional elements in the cytosolic face of the channel. Therefore, we tested whether internal TEA prevents the closing of the slow inactivation gate as it does with the activation gate in voltage-gated K channels (Armstrong, 1966).

To measure the internal TEA effects on slow inactivation and deactivation kinetics, it is necessary to gain perfusional access to the cytosolic side of the channel. We used the COVC technique (Taglialatela et al., 1992) instead of excised membrane patches because dramatic changes in the inactivation kinetics have been observed with the latter technique (Chen et al., 2000; Oliva et al., 2005; see Discussion). With the purpose of obtaining a larger signal to monitor the deactivation tails of current, we increased the K^+-driving force by elevating the external K^+ concentration to 25 mM instead of the 2 mM used in TEVC recordings. This operation did not introduce significant modification to either the inactivation kinetics or the inactivation extent at the end of a 15-s pulse (see Fig. 10 A). Thus, with COVC the slow inactivation kinetics were indistinguishable from those obtained with the TEVC technique.

After establishing the voltage-clamp configuration, we waited >20 min to allow the current to stabilize before starting with the voltage protocols and the perfusion of an internal solution containing 5 mM TEA (vertical dashed line in Fig. 5, C–E; see Materials and methods for details). The solution exchange was monitored once every minute with the voltage-pulse protocol depicted in Fig. 5 A. We analyzed three variables in each current trace: (1) the amplitude at 0 and +40 mV to examine the extent of the blockade by TEA (Fig. 5 C), (2) the time constant of the current decay during a 15-s pulse to 0 mV to follow the effect of TEA on the inactivation kinetics (Fig. 5, A, right, and D), and (3) the time constant of deactivation at −110 mV after the 20-ms pulse to +40 mV (Fig. 5 A) to track the interference of TEA on the deactivation kinetics (Fig. 5, B and E). The letters a, b, and c in Fig. 5 indicate various stages during the progress of the experiment (see figure legend for details). At the end of the solution exchange, both deactivation and inactivation time constants had increased dramatically, approximately four- and twofold, respectively. Although the effect of the internal TEA on the deactivation kinetics was as expected (Armstrong, 1966), its effect on slow inactivation is not anticipated by the classical C inactivation mechanism (Choi et al., 1991). To illustrate the dramatic delay introduced by internal TEA on the slow inactivation kinetics, we show representative traces in response to a 60-s pulse to −15 mV (Fig. 6) before

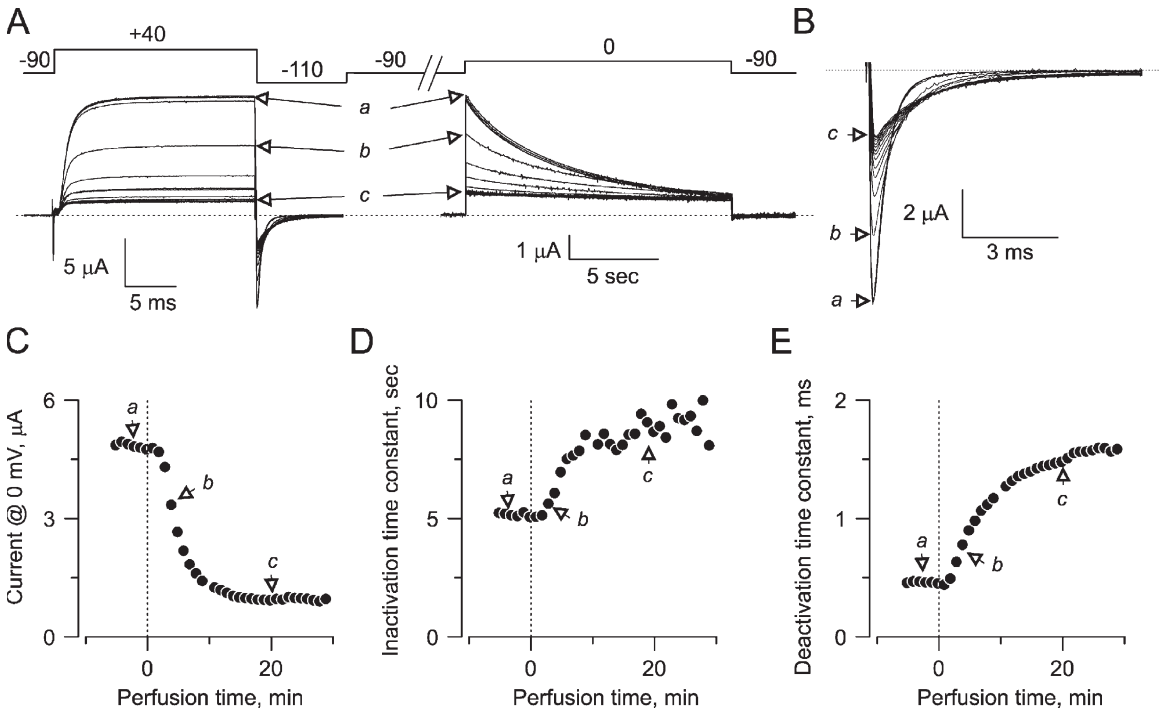

Figure 5. Diffusional perfusion of internal TEA. (A) COVC current traces elicited by a protocol depicted at the top of the figure. The membrane voltage was held at −90 mV, and voltage was pulsed for 20 ms to +40 mV. Voltage was then returned to −110 mV to induce inward tails of currents. Then, at a different clock rate, a 15-s pulse to 0 mV was applied to assay inactivation kinetics. The variation between traces corresponds to different stages in the diffusional perfusion of internal 5 mM TEACl added on top of the cytosolic solution. Letters a, b, and c indicate traces acquired 3 min before and 3 and 20 min after the beginning of the perfusion of TEA, respectively. For this type of recording, 25 mM Na^+ was equivalently replaced by K^+ in the external solution to increase the size of the inward tails of currents. (B) The size and kinetics of the tails of currents allow monitoring of the progress of the internal perfusion of TEA and its effect on the deactivation kinetics (see main text for details). The traces shown correspond to an enlargement of the currents recorded at −110 mV in A (left). Single exponential functions were fit to the currents (see Fig. 7). (C) Time course of inhibition by 5 mM of internal TEA of the ionic current elicited by a 0-mV pulse. The vertical dashed line indicates the moment at which we changed the composition of the solution at the internal chamber to initiate the diffusional perfusion of 5 mM TEACl into the cytosolic face. (D and E) Time course of the effect of the internal perfusion of TEA on the time constants of slow inactivation and deactivation (see main text for details), respectively.

(thin trace) and at the end of an internal 5-mM TEA perfusion experiment (thick trace). The extent of the slowdown is such that the current traces intersect each other, illustrating the paradoxical fact that the K currents recorded in the presence of the pore blocker are larger than they are in its absence. Such a result shows that this quaternary ammonium antagonizes the inactivation forward rate while the backward rate remains mostly unaffected (see below).

It is technically difficult to test more than a single intracellular TEA concentration in the same oocyte because of the time-dependent deterioration of the voltage-clamp recording. As an alternative, we assessed the extent of the interference of TEA with the slow inactivation kinetics by following the progress of ionic current inhibition. This measure provided a rough approximation of the average TEA dilution in the vicinity of the K channels. Fig. 7 plots the apparent deactivation rate at −110 mV (Fig. 7, A and B) and the inactivation rate at 0 mV (Fig. 7, C and D) as a function of the unblocked fraction of channels. At −110 mV, the tail current relaxations were fitted to single exponential functions, and the fractional unblocked currents (a/a_o in Fig. 7 A)

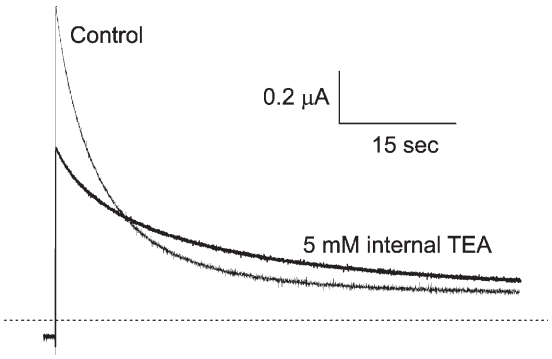

Figure 6. Slow inactivation retardation by internal TEA produces crossing over of the current traces in *Shaker* IR. Two ionic current traces elicited by a 60-s pulse to −15 mV obtained before (thin line) and 40 min after (thick line) the beginning of the perfusion of internal TEA. The antagonism of TEA on slow inactivation is such that at the end of a 60-s pulse, the total ionic currents in the blocked channels is larger than that in the unblocked one.

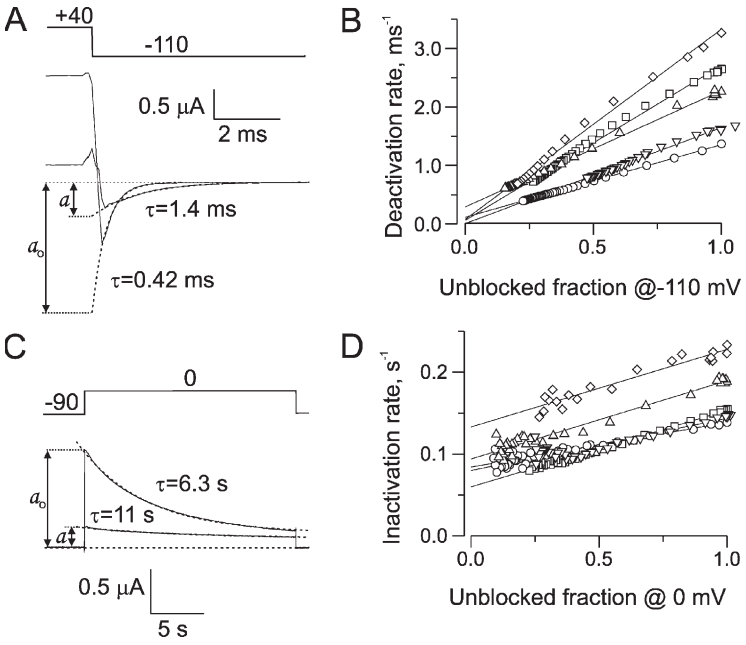

Figure 7. Internal perfusion of TEA delays deactivation and slow inactivation in *Shaker* IR. (A) Elements of the analysis of the effect of internal TEA on the tails of currents measured at −110 mV. As examples, the first and last traces of the experiment in Fig. 5 are shown. Current deactivations were fit to a single exponential function, and the time constant is shown on top of each trace (discontinuous lines). The amplitudes a_o and a are extrapolations of the curves fit to the peak of the preceding capacitive transient, in which a is the amplitude of a given trace and a_o is the amplitude of the first one. The ratio a/a_o is the unblocked fraction at −110 mV. (B) Plot of the deactivation rate as a function of the unblocked fraction of currents for five different oocytes. Continuous lines are the linear regressions used to estimate the values of α and β (see main text). (C) Elements of the analysis of the effect of TEA on the ionic currents measured at 0 mV. Fitted single exponential functions are shown as discontinuous lines on top of two example traces with the times constants shown, while a and a_o have the same meaning as in A. (D) Plot of the slow inactivation rate as a function of the unblocked fraction of currents for the five oocytes shown in B. Identical symbols in B and C correspond to data from the same cell. Continuous lines are linear regressions to estimate the values of TEA-dependent inactivation constant.

were obtained from the ratio of extrapolated amplitudes to the peak of the preceding capacitive transient. Fig. 7 B plots the reciprocals of deactivation time constants (deactivation rate in ms^{-1}) versus the fractional unblocked current for five oocytes. Similarly, current decays during a 15-s pulse to 0 mV were fitted to monoexponential functions, and the fractional unblocked currents (a/a_o in Fig. 7 C) were measured at the peak. Fig. 7 D plots the reciprocal of the time constants (apparent inactivation rate in s^{-1}) against the fractional unblocked current at 0 mV for the same oocytes shown in Fig. 7 B. As expected from the classical "foot in the door" mechanism, Fig. 7 B shows a linear relationship between the apparent deactivation rate and the fractional unblocked current during the perfusion of the oocytes. Considering the roughness of the procedure we used for diffusional perfusion of the oocyte intracellular face, it is somehow surprising that such a well-behaved linear relationship was obtained.

The foot in the door mechanism can be summarized by the following simple scheme:

$$C \underset{\alpha}{\overset{\beta}{\rightleftarrows}} O \longleftrightarrow B_{in}$$

SCHEME 2

where α and β are the opening and closing rates, respectively. A simple general formula to describe how the deactivation rate, δ, depends on the fraction of unblocked channel at −110 mV ($U_{(-110)}$) is the following:

$$\delta = \beta \times U_{(-110)} + \alpha. \quad (1)$$

For the five experiments shown in Fig. 7, β averaged 2.1 ± 0.32 ms^{-1}, whereas α was 0.022 ± 0.056 ms^{-1}, illustrating the fact that at −110 mV the closing rate dominates the kinetics of deactivation.

The apparent macroscopic inactivation rate also increased linearly with the unblocked fraction of channels at 0 mV (see Fig. 7 D). With a slope of 0.053 ± 0.0071 s^{-1} ($n = 5$), these data suggest the existence of a slow inactivation gate also operating in the foot in the door manner. On the other hand, the extrapolation to $U = 0$ departed significantly from the origin of the graph, revealing a large $[TEA]_{in}$-independent component of 0.083 ± 0.0049 s^{-1} in the slow inactivation kinetics. Such a component could result from the contribution of the $[TEA]_{in}$-insensitive rates of recovery added to other $[TEA]_{in}$-insensitive inactivation rates such as the classical C inactivation (Choi et al., 1991). Therefore, an empirical description of the inactivation rate, I, as a function of the fraction of unblocked channels at 0 mV is:

$$I = s \times U_{(0)} + i, \quad (2)$$

where s is the $[TEA]_{in}$-sensitive rate and i is the compound rate of all $[TEA]_{in}$-insensitive inactivation and recovery rates. Accordingly, in addition to interfering with the activation gate, $[TEA]_{in}$ also interferes with the slow inactivation gate in an equivalent fashion. Thus, in our experimental conditions, a major portion of the inactivation kinetics is dominated by a cytosolically exposed gate.

In contrast to *Shaker* IR, when *Shaker* IR T449S channels are subject to the internal 5-mM TEA solution

exchange in experiments similar to those described in Fig. 5, the inhibition of the current (Fig. 8 A) and the slowing down of the deactivation currents are evident (Fig. 8 B). However, a very modest, if any, effect is observed on the inactivation kinetics (Fig. 8 C, open circles). We consistently observed this type of behavior in all five oocytes expressing this *Shaker* variant that were subject to the internal TEA perfusion protocol. Such a result is expected if the classical C-type inactivation mechanism dominates the inactivation of this *Shaker* variant (Choi, et al., 1991; López-Barneo et al., 1993; Jerng and Gilly, 2002).

We measured the effect of internal TEA on the steady-state voltage dependence of inactivation in the *Shaker* IR channels (Fig. 9) by performing the voltage protocol depicted in Fig. 2 before, and at the end of, the perfusion with the 5-mM TEA internal solution. As a control for the dialysis produced solely by the perfusion of the internal solution, we also measured the voltage dependence of steady-state inactivation 30 min after the perfusion of a TEA-free internal solution. After 30 min of perfusion with the control TEA-free solution, we observed a $\Delta V_{0.5} = -2.56 \pm 0.92$ ($n = 3$) in the Boltzman distribution fit, which is statistically indistinguishable from -3.24 ± 0.95 mV ($n = 5$) obtained from TEA-perfused oocytes (P = 0.65; two-tailed t test). Thus, if 5 mM of internal TEA introduces a shift along the voltage axis on the voltage-dependent steady-state slow inactivation, the shift is smaller than our detection limit of 3.1 mV (with respect to the shift produced by the dialysis). Because of the large impact of internal TEA on the inactivation kinetics, such a small effect is somehow surprising.

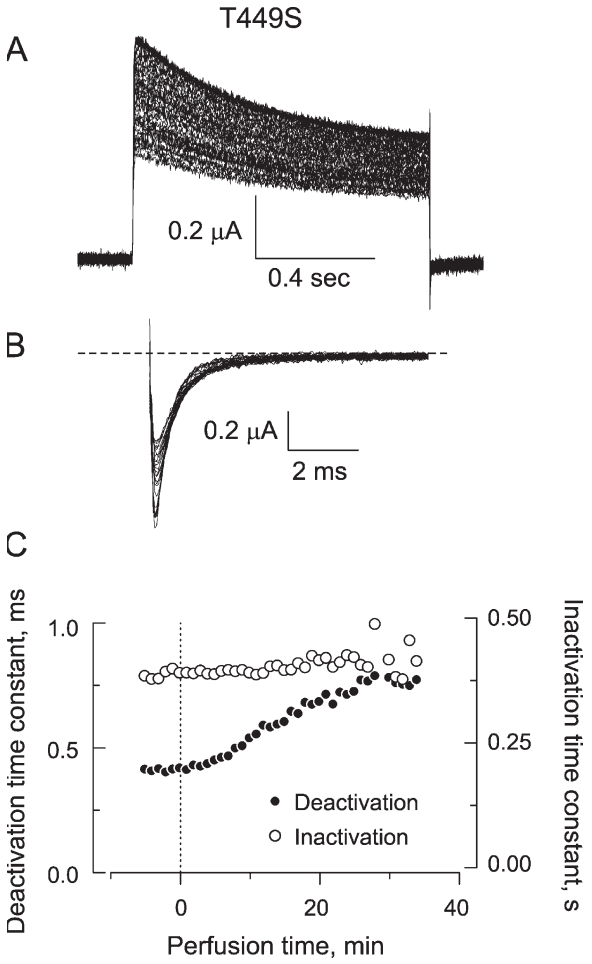

Figure 8. Inactivation kinetics in *Shaker* IR T449S is not slowed by internal TEA. (A) COVC current traces elicited by a 1-s pulse to 0 mV during the internal diffusional perfusion of 5 mM TEA. (B) Tails of currents are slowed as the ionic current inhibition progresses. (C) Time course of the change on the deactivation and inactivation kinetics. The vertical dashed line indicates the moment at which we changed the composition of the solution at the internal chamber to initiate the diffusional perfusion of 5 mM TEACl into the cytosolic face on the oocyte.

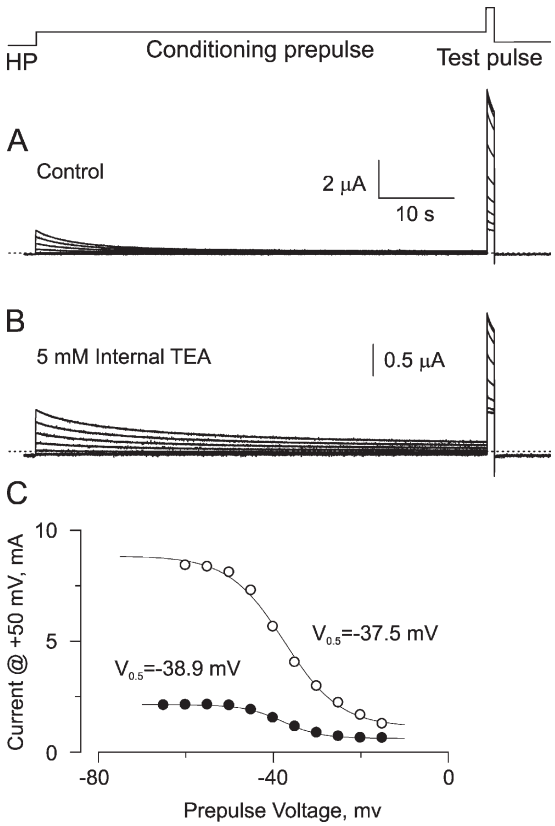

Figure 9. Voltage dependence of *Shaker* IR channel availability in the presence of internal TEA. (A) Ionic currents in the absence of TEA elicited using the protocol schematized at the top of Fig. 2 in COVC. (B) Similar traces obtained after 40 min of diffusional perfusion of internal 5 mM TEA. (C) Comparison of the peak current amplitude at the test voltage pulse for the control traces shown in A (open circles) and after the 40-min perfusion of TEA traces in B (filled circles). The continuous lines are fits to a Boltzman distribution function with the half inactivation voltages depicted in the figure using an effective valence of $z = -4.6$ e_o for the control traces and $z = -5.81$ e_o for the traces with TEA. The holding voltage was −90 mV. Discontinuous lines in A and B indicate zero current level.

A small negative shift in the voltage-dependent channel availability might be expected if the internal TEA-sensitive inactivation was preferentially accessed after a large fraction of the gating charge had been activated, or if the recovery rate was also slowed down by internal TEA.

The Effect of Internal and External TEA on the Kinetics of Recovery from Inactivation

We compared the kinetics of recovery from inactivation using a standard two-pulse protocol with a variable interpulse interval (Fig. 10). We applied a 15-s pulse to 0 mV to produce a significant inactivation followed by a second test pulse to 0 mV after a variable, interpulse interval ranging from 0.01 to 6 s at −90 mV. The effects of external TEA and internal TEA on recovery were assessed with TEVC and COVC techniques, respectively. The top of Fig. 10 A shows that the families of current traces obtained with both voltage-clamp techniques are nearly identical at the onset as well as in the recovery from inactivation. The time course of recovery was characterized by two well-separated kinetic components of similar amplitude. The time constants for the fast and slow components were ∼30 ms and ∼2 s, respectively (open symbols in both panels of Fig. 10 B). The presence of these two components in the recovery kinetics makes a clear indication that *Shaker* IR K channels have at least two kinetically separate inactivated states (see also, Olcese et al., 1997; Basso et al., 1998; Klemic et al., 2001; Oliva et al., 2005). The addition of 40 mM TEA, at constant ionic strength, to the external solution increased the proportion of the fast recovery component to ∼65% (Fig. 10 A and filled circles in the left panel of B), whereas the addition of 5 mM of internal TEA had the opposite effect, reducing it to ∼34% (Fig. 10 A and filled circles in the right panel of B). These results indicate that when the channels are internally blocked by TEA, they preferentially inactivates to a state having the slower recovery kinetics, possibly the C-inactivated state. Conversely, when channels are blocked from the outside,

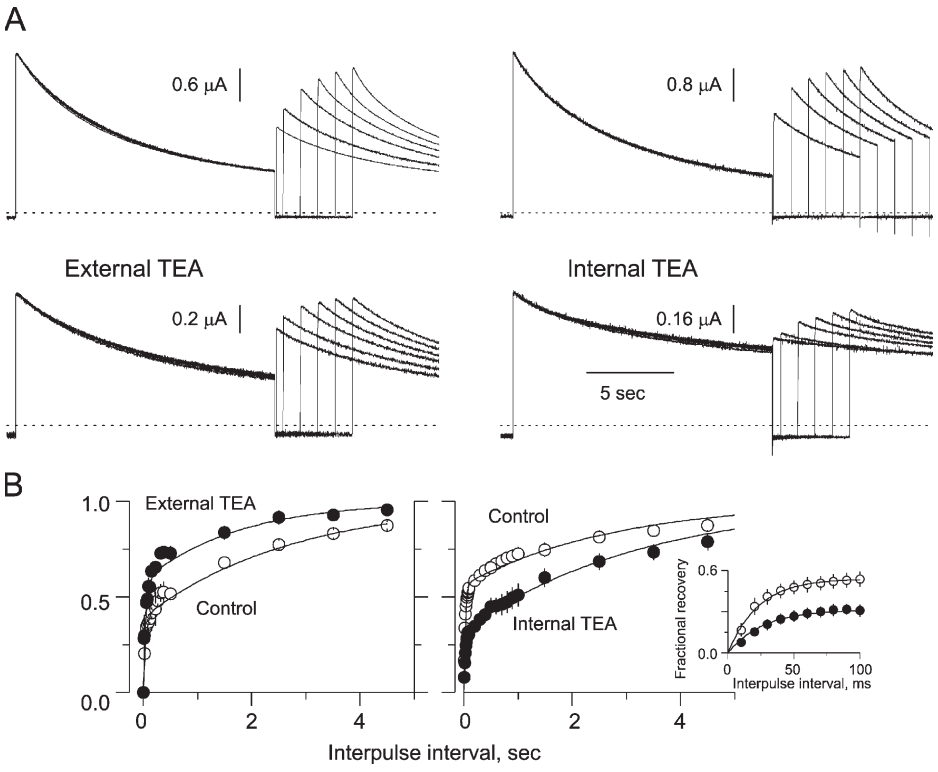

Figure 10. Effect of internal and external TEA in the kinetics of recovery from inactivation. (A) Ionic current traces in response to a two-pulse protocol used to measure the rate of recovery from inactivation. From a holding potential of −90 mV, a 15-s conditioning pulse to 0 mV was applied to induce a significant amount of inactivation. Then, after a variable interpulse interval ranging from 10 to 5,000 ms at −90 mV, a second test pulse was applied to measure at the peak the amount of recovery. The top panels show the control traces for TEVC (left) and COVC (right). Note the similarity in the currents obtained using these two modes of recording. The two-pulse recording in the presence of external TEA at 40 mM (left) and after ∼40 min of internal perfusion of 5 mM TEA (right) are shown, rescaled to accentuate the differential effect of TEA on the kinetic component of the recovery (note the different scale bar). (B) Normalized fractional recovery before (open circles) and after (filled circles) the perfusion of external (left) and internal TEA (right). The difference between peak current at the test pulse and the current at the end of the conditioning pulse was normalized according to the relation: $1-[(f_{test}-1)/(f_{end}-1)]$, where f_{test} and f_{end} are the fractional current at the test (peak) and at end of the conditioning pulse, respectively. The solid lines are fits to a two-exponential function of the form $f(t) = 1 + A_f \times \exp(-(t-t_o)/\tau_f) + A_s \times \exp(-(t-t_o)/\tau_s)$, where τ_f and τ_s are the time constants of both kinetic components of the recovery, $-A_f$ and $-A_s$ are the fractional amplitude of each component, and t_o is the end of the conditioning pulse. The parameters used for fitting the data on the left panel are: $A_f = -0.39 \pm 0.04$, $\tau_f = 40 \pm 8.4$ ms and $A_s = -0.61 \pm 0.02$, $\tau_s = 2{,}750 \pm 274$ ms for the control, and $A_f = -0.58 \pm 0.07$, $\tau_f = 45 \pm 13$ ms, and $A_s = -0.42 \pm 0.05$, $\tau_s = 1{,}740 \pm 550$ ms for the 40 mM external TEA; for the right panel data they are: $A_f = -0.53 \pm 0.04$, $\tau_f = 29 \pm 4$ ms and $A_s = -0.44 \pm 0.01$, $\tau_s = 2{,}800 \pm 320$ ms for the control, and $A_f = -0.34 \pm 0.05$, $\tau_f = 34 \pm 10$ ms and $A_s = -0.67 \pm 0.03$, $\tau_s = 3{,}500 \pm 400$ ms for the internally perfused TEA. (Inset) Expanded time scale for the recovery data during the first 100 ms. For this time interval, data were fit to a single exponential function with time constant, $\tau = 23 \pm 3$ ms, and amplitude, $A = 0.54 \pm 0.05$ for the control, and $\tau = 26 \pm 13$ ms, with $A = 0.3 \pm 0.03$ for data in the presence of TEA. Each data point in the figure corresponds to an average of five to eight different oocytes.

they inactivate preferentially to a state having the faster recovery. Thus, the outcome of these experiments indicates that the internal TEA-sensitive inactivation is the one having the faster recovery.

Because the current decays presented in Fig. 6 suggested that the recovery rate is poorly sensitive to internal TEA, we did a detailed study to test its effects on the magnitude of the faster recovery rate. The inset in the right panel of Fig. 10 B illustrates that, in fact, TEA did not significantly affect the recovery time constants but instead altered the proportion of each of the components. As shown previously for the *Shaker* K channel family, these results also indicate that within the time scale of the experiments outlined in Fig. 10, there is little exchange between both types of inactivated states (Basso et al., 1998; Klemic et al., 2001; Kurata et al., 2005).

The Internal TEA Alters the Gating Charge Movement in the Inactivated State

Olcese et al. (1997) proposed that slow inactivation introduces a large negative shift to the curve describing the voltage dependence of the charge movement, as if inactivation locked the voltage sensor in a different conformation, requiring the application of more negative voltages to make the charges return to the resting state. These authors proposed that in *Shaker* IR, the voltage sensor moves in two parallel energy paths associated with the normal and the slow inactivated gating (Q1 and Q2, respectively). Such exchange between Q1 and Q2 also occurred in the constitutively C-inactivated *Shaker*–IR-W434F, suggesting that a significant fraction of the charge exchange would not be functionally linked to C inactivation. We tested if the internal perfusion with TEA alters Q1-Q2 conversion by measuring its effect on the voltage dependence of gating charge movement. To measure the gating currents in *Shaker* IR, we removed the K^+ from the internal and the external solutions, and added 5 μM agitoxin II externally to block ionic currents (Hidalgo and MacKinnon, 1995). Fig. 11 A shows leakage- and capacitance-subtracted gating currents from an oocyte equilibrated with NMG-MES internal solution before (left) and ∼70 min after the beginning of the perfusion with NMG-MES plus 5 mM TEA (right). Gating currents were elicited by 20-ms pulses from two different holding voltages: from −90 mV to observe the normal gating path between closed and open states, and after 5 min at 0 mV to observe the slow inactivated gating path. As internal perfusion with 5 mM TEA progressed, inward-going gating currents became progressively slower and smaller, whereas outward-going currents did not changed noticeably, illustrating that TEA interfered only with the closing of the activation gate. Fig. 11 B shows the outward charge movement as a function of the pulse voltage from both holding voltages (Q-V relation) before (open symbols) and after 70 min of internal TEA perfusion (filled symbols). With the holding potential at −90 mV, TEA introduced a negligible shift to the Q-V relation (Fig. 11 B, circles), indicating that although the channels were closed, TEA interfered weakly with the charge movement.

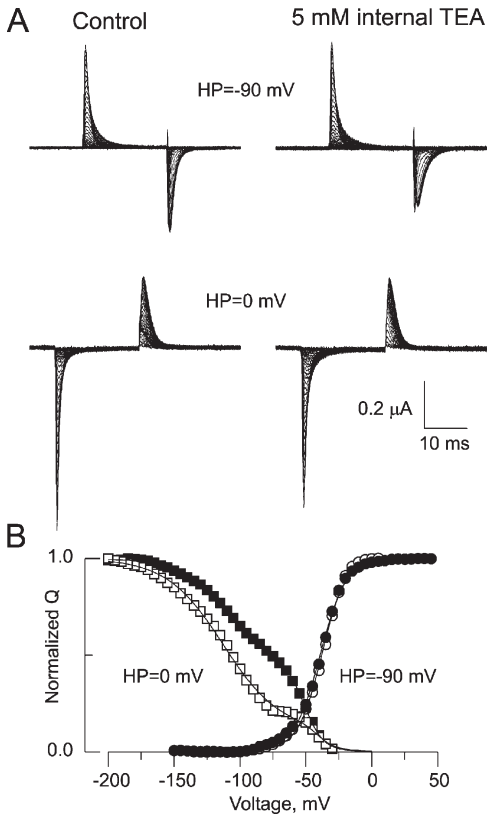

Figure 11. Effect of internal TEA on the gating currents. (A) Gating currents of *Shaker* IR channels from a holding potential of −90 mV (top) or 0 mV (bottom), before (left) or 70 min after (right) the beginning of the diffusional perfusion of 5 mM TEA. To be as close as possible to inactivation at equilibrium, the oocyte was kept at a 0-mV holding potential for 5 min before the beginning of each family of voltage pulses. To minimize fast recovery during pulses from 0 mV (see Fig. 10), we kept the pulse duration to 20 ms, a duration balancing the need for a reliable estimation of the base line and recovery. Gating current sizes were stable during the experiments. Although traces at left and right are separated by >70 min, the outward-going gating currents changed in <10%. (B) Outward-going gating charge from either a holding voltage of −90 mV (circles) or 0 mV (squares). The charge measurement made 70 min after the perfusion of TEA (filled symbols) shows a marked disparity to the controls (open symbols) only for the pulses from a holding potential of 0 mV. Q-V relation elicited from a holding potential of −90 mV were fitted to a single Boltzman distribution function with the following parameters: $V_{0.5}$ = −37.7 mV with z = −2.81 e for the control measurements and $V_{0.5}$ = −39.0 mV with z = −2.63 e with internal TEA. On the other hand, the Q-V curves elicited from a holding potential of 0 mV were fitted to a two-Boltzman distribution function representing Q1 and Q2 as in Olcese et al. (1997). Parameters used to fit the control charge displacement are: $V_{0.51}$ = −40.4 mV with z_1 =4.27 e having a fractional area of 0.11; and $V_{0.52}$ = −107 mV with z_1 = 1.33 e. Those for the charge displaced in the presence of internal TEA are: $V_{0.51}$ = −50.8 mV with z_1 =3.75 e having a fractional area of 0.59, and $V_{0.52}$ = −113 mV with z_1 =1.2 e.

Additionally, internal TEA shifted the Q-V curve for inward-gating current ~5 mV in the negative direction, revealing the expected interference with the closing gate (not depicted). However, with the holding voltage at 0 mV, a visible distortion in the Q-V relation was observed (Fig. 11 B, squares). Following Olcese et al. (1997), we fitted a two-Boltzman distribution function to the Q-V relation, with Q1 corresponding to the normal gating from the closed state and Q2 corresponding to the gating within the slow inactivated pathway. In our measurements, internal TEA increased Q1 from ~10 to ~45%, demonstrating its interference with the Q2 component. Because the Q1-Q2 also interconvert in the constitutively C-inactivated *Shaker* IR mutants W434F, D447E, and D447N/T449V (Seoh et al., 1996; Olcese et al., 1997), these results further suggest that the slow inactivation antagonized by TEA can, in part, be associated with the Q2 component of the gating charge voltage dependency.

DISCUSSION

In *Shaker* K channels, the removal of the (usually fast) N-type inactivation uncovers a distinct and kinetically slower inactivation, which was termed C-type inactivation (Hoshi et al., 1991). The description of the classical C inactivation mechanism implies a localized constriction at the external half of pore. This picture emerged because external TEA, but not internal TEA, retards inactivation kinetics in a mutually exclusive manner, consistent with Scheme 1 (Choi et al., 1991), and is antagonized by the addition of external K^+ (López-Barneo, et al., 1993; Baukrowitz and Yellen, 1996; Molina et al., 1998). In this picture, the occupancy of an externally accessible binding site by either K^+ or TEA prevented the closure of the inactivation gate as a foot in the door. In agreement with these observations, residue 449, located at the external pore entrance, when substituted by cysteine, can coordinate divalent metals with several thousand–fold higher affinity in the slow inactivated state than in the open state (Yellen et al., 1994). This pore constriction must be very localized, even within the pore, because inactivated channels bind pore-occluding scorpion toxins as well as closed channels (Liu et al., 1996), and, on the other hand, pore-occluding peptide toxins do not antagonize with inactivation (Oliva et al., 2005). This clear picture on how slow inactivation occurs was constructed mostly from experiments done with the patch-clamp technique. However, a more complicated and blurry picture of slow inactivation arose with the use of other electrophysiological techniques applied to *Shaker* K channels in whole oocytes. Gating current measures indicated that during slow inactivation, the voltage sensor is arrested in a very stable set of conformations (Olcese et al., 1997). Although these results involved other functional loci in the slow inactivated conformational state, they did not affect the localized pore collapse hypothesis as long as slow inactivation occurred after the voltage sensor had reached the active conformation, near the open state. However, the non K-conducting *Shaker* mutant W434F, a constitutively inactivated channel (Yang et al., 1997), also exhibited this type of charge arrest, indicative of, at least, two separate slow inactivation mechanisms. Fluorescent probes attached to either S4 or the external vestibule also reported two, possibly sequential, conformational changes associated with slow inactivation (Cha and Bezanilla, 1997; Loots and Isacoff, 1998). Thus, P inactivation, a term coined by De Biasi et al. (1993) to account for the effect of mutations in the pore loop of Kv2.1, was assumed to be an initial pore collapse, whereas C inactivation was a more generalized stabilization of the nonconducting conformation. The experimental difficulties for a clear phenomenological dissection between these processes led to the use of the P/C inactivation terminology (see for example Chen et al., 2000; Claydon et al., 2007). Several other results complicated the mechanistic interpretation of slow inactivation in *Shaker* K channels. Unlike the experiments done with patch clamp (Choi et al., 1991; Molina et al., 1998), slow inactivation was nearly insensitive to external TEA in TEVC experiments (Yang et al., 1997). Moreover, in clear opposition to the expectations from the classical C-type inactivation paradigm, inactivation at voltages near zero appeared to be enhanced by external application of TEA or high K^+ (Klemic, et al., 2001). At more positive voltages, macroscopic inactivation resembled more the classical C-type inactivation, suggesting two separate coexisting inactivation pathways. Klemic et al. (2001) suggested that high positive voltage favors C-type inactivation, whereas moderate depolarization favors an inactivated conformation visited from partially activated closed states. Thus, at voltages near zero, both types of inactivation are present and inactivation is maximal, resulting in a U-shape for the voltage dependence. For this closed-state visited inactivation, these authors coined the term U-type inactivation.

Structural as well as molecular dynamic studies on bacterial potassium channels have provided molecular pictures for the constriction in the selectivity filter that could account for the classical C-type inactivation (Zhou et al., 2001b; Bernèche and Roux, 2005; Cordero-Morales et al., 2007). But a molecular picture for the other type(s) of coexisting slow inactivation(s) in *Shaker* K channels is lacking. Here, the two-pulse experiments outlined in Fig. 10 were particularly informative to show relevant similarities between the internal TEA-sensitive slow inactivation and U-type inactivation (Klemic et al., 2001). As U-type inactivation, the internal TEA-sensitive inactivation is associated with the fast component of the recovery, a component enhanced by external TEA (and here, diminished by internal TEA; Fig. 10). Also, as U-type inactivation, this component did not interconvert with C-type inactivation.

The results reported here are largely consistent with the idea that U-type inactivation is sensitive to internal TEA.

Shaker IR Slow Inactivation in Whole Oocyte

In open contradiction to the experiments describing the basic features of C inactivation, here we report that in whole oocytes, *Shaker* IR slow inactivation is weakly sensitive to external TEA, but markedly sensitive to internal TEA (compare Figs. 1 and 5). We do not understand the basis for such differences with the experimental results from the Yellen and Aldrich laboratories, except that the classical experiments to describe C- type inactivation were made with patch clamp, most of them in cell-free membrane patches (Choi et al., 1991; Hoshi et al., 1991; López-Barneo et al., 1993; Yellen et al., 1994), whereas ours were made with whole oocyte recording techniques. Profound kinetic alterations in slow inactivation take place when membrane patches are removed from cells to obtain the outside-out configuration; for example, inactivation kinetics become three- to fourfold faster and more complete (Chen et al., 2000; Oliva et al., 2005). Inactivation can be appreciably antagonized by external TEA only after patch excision, and in outside-out patch clamp, recovery from inactivation is mono-exponential with a time constant that compares to the slow component of recovery seen in the present work (Oliva et al., 2005). Thus, while in excised membrane patches the classical C-type inactivation mechanism dominates the slow inactivation (Choi et al., 1991), in whole oocytes, and in cell-attached patch clamp, a slower and kinetically complex inactivation prevails (see for example: Olcese et al., 1997; Yang et al., 1997; Klemic et al., 2001; Oliva et al., 2005; Klement et al., 2008).

Because the classical C inactivation is slowed down by high external K^+, local K^+ accumulation at the extracellular oocyte membrane infoldings could explain the slower inactivation observed in whole oocyte recordings. However, in our experiments in whole oocytes, inactivation kinetics was independent of the size of the ionic currents within a range of two orders of magnitude (0.1–10 μA), and nearly independent of the external K^+ (2–25 mM). Moreover, recording of the nonconducting W434F *Shaker*-IR in whole oocyte, in which potassium accumulation is not an issue, charge immobilization and remobilization associated to slow inactivation closely match the kinetics of inactivation and recovery of the ionic currents (Olcese et al., 1997). In our hands, regardless of the number of channels in the patch (from one to thousands), slow inactivation kinetics remain nearly unchanged in outside-out patch-clamp measurements (García et al., 1999; Naranjo, 2002; Oliva et al., 2005).

Although K^+ accumulation could specifically slow down the C-type component in a K channel having multiple inactivating pathways, this hypothesis is insufficient to explain the overall slower inactivation kinetics observed in whole oocyte because, even with 100 mM external K^+, inactivation time constants in outside-out patches are 25–50% of those seen in whole oocytes (López-Barneo et al., 1993; Baukrowitz and Yellen, 1996; Molina et al., 1998). The K^+ accumulation hypothesis is also inadequate because under our recording conditions, potassium accumulation would lead to a moderate increase in the rate of inactivation (Klemic et al., 2001). Instead, we favor the idea that multiple inactivation processes coexist in *Shaker* IR, and the type of inactivation dominating slow inactivation kinetics could be determined by experimental manipulations affecting cell integrity, as occurs after patch excision. We propose that in whole oocytes, in addition to the C inactivation gate, the internal TEA-sensitive slow inactivation contributes significantly to the slow inactivation kinetics. What makes *Shaker* IR K channels inactivate mostly in the classical C-type mechanism after patch excision remains to be solved.

A Single TEA Binding Site?

The correlation between the introduced delay in both the slow inactivation and the closing of the activation gate promoted by internal TEA could result from the binding of this quaternary ammonium to the ionic pathway in the open channel, interfering with both processes. This is the most simplistic interpretation. However, TEA could be binding to two different sites, one governing the activation gate and the other controlling the slow inactivation gate. Because neither gates close while TEA is bound to the channel, as in a foot in the door mechanism, the involvement of a single site seems more likely. In such a case, the affinity and voltage dependence of the TEA binding site that delays inactivation should be the same as the one retarding the closing of the activation gate, both being identical to the TEA binding site that interrupts ionic current.

The drawback of the internal perfusion experiments for measuring affinity for TEA (see Fig. 5) is that ordinarily we could perfuse thoroughly only with a single TEA concentration. A direct estimation of the TEA-dissociation constant of the binding site(s) governing deactivation and inactivation requires testing at equilibrium several TEA concentrations in the same oocyte. Such experiments are difficult to achieve because it usually takes ∼1 h for the internal perfusion to reach a plateau, and oocytes in the cut-open configuration seldom survive more than 2 h. However, assuming that during the progress of the internal perfusion TEA occupancy of the channels remains constant during the ∼16 s that spans the application of deactivation and inactivation protocols shown in Fig. 5 A, we can obtain the ratio between the dissociation constants governing both processes. This invariance in the TEA concentration would be a bold assumption at the beginning of the perfusion because the rate of change in the current inhibition is

the largest. However, as seen in Fig. 5 C, only a few points, usually <10, show inhibition corresponding to a change of >10% in the occupancy between consecutive pulses (arrows *b* in Fig. 5). Thus, the assumption is reasonably correct for a large majority of the data collected with the internal TEA perfusion protocol (arrows *c* in Fig. 5). As a first approximation to obtain the ratio between both dissociation constants, we assumed homogeneous, although unknown, distribution of [TEA] under the voltage-clamped casket in the COVC. This assumption is approximately correct given that the tail relaxations could be closely fit by a single exponential function (Fig. 7 A). We also assumed that the pore binding kinetics are much faster than channel gating. With these assumptions, the unblocked fractions of currents at 0 and −110 mV are, respectively:

$$U_{(0)} = (1+[\mathrm{TEA}]/K_{\mathrm{D}(0)})^{-1} \text{ and } U_{(-110)} = (1+[\mathrm{TEA}]/K_{\mathrm{D}(-110)})^{-1},$$

where $K_{D(0)}$ and $K_{D(-110)}$ are the dissociation constants for both blockade equilibriums. By replacing both expressions in Eqs. 1 and 2 in Results, we obtain:

$$\delta = \beta \times (1+[\mathrm{TEA}]/K_{\mathrm{D}(-110)})^{-1} + \alpha$$

and

$$I = s \times (1+[\mathrm{TEA}]/K_{\mathrm{D}(0)})^{-1} + i.$$

As long as [TEA] remains constant between the deactivation and inactivation measurements, solving for [TEA] in both expressions, we obtain:

$$m \times (\delta_0 - \delta)/(\delta - \alpha) \approx (I_0 - I)/(I - i),$$

where $m = K_{D(-110)}/K_{D(0)}$ and δ_0 and I_0 are the deactivation and inactivation rates in the absence of TEA. Assuming that α is very small (see Fig. 7), we obtain the following expression:

$$s/(I - i) \approx \mathrm{m} \times (\delta_0 - \delta)/\delta + 1.$$

The slope of $s/(I\text{-}i)$ against $(\delta_0-\delta)/\delta$ is m the ratio of the dissociation constants. Fig. 12 A shows that TEA sensitivity of the site controlling the inactivation gate correlates with that of the one controlling the closing rate. On the other hand, using similar arguments, we can arrive to the following expression for the TEA-induced inhibition at 0 and −110 mV:

$$[(a_o - a)/a]_{(0)} = m \times [(a_o - a)/a]_{(-110)}.$$

Fig. 12 B plots the amount of current inhibition at 0 mV versus the amount at −110 mV. The straight line is the ratio between the dissociation constants for the pore blockade.

Both values for m in Fig. 12 are around 1, indicating that the K_Ds for both processes have similar voltage dependencies. Given the uncertainty of the internal TEA distribution, and the true position of the zero current level in the COVC experiments (see Materials and methods), these determinations seek internal experimental consistency rather than pretending to measure the true voltage dependence of the TEA binding equilibrium. Similar voltage dependencies suggest a single TEA binding site regulating inactivation and deactivation. Such a binding event of pore blockade by TEA would not only control permeation, but also deactivation and slow inactivation. In agreement with this proposal, and with the current structural picture of the binding site for tetraalkyammonia in the internal cavity of the pore (Zhou et al., 2001a), all the effects promoted by internal TEA examined in this paper require that it binds to the open conformation, a conformation that, to our knowledge, has a single cytosolically exposed TEA binding site, the pore-occluding site.

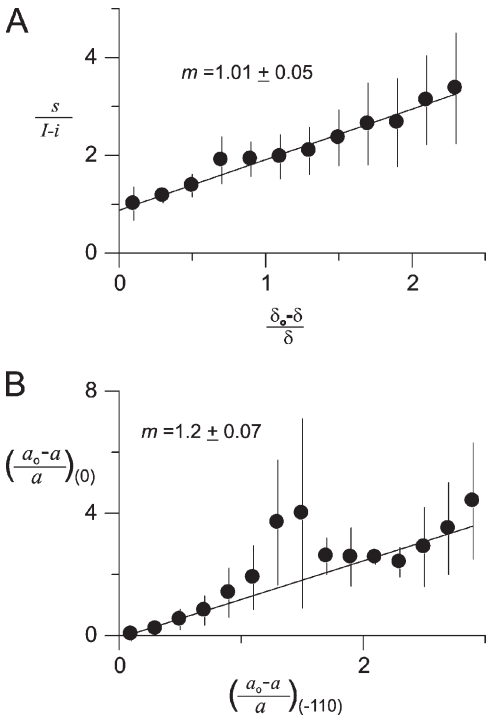

Figure 12. The operational voltage dependence of the blockade. (A) Effect of internal TEA on the deactivation versus inactivation. (B) Current inhibition by internal TEA at −110 mV versus the inhibition at 0 mV. See details in the main text. Abscissa data were binned every 0.2 units. The average ± SEM versus the central values of the bin are plotted. The plotted data were clipped at the extreme values; however, >90% of the total data points are represented for each case. In A, this 90% of the data points includes up to 80% of ionic current blockade by internal TEA, whereas in B data include up to a 3.5-fold increase in the deactivation time constant.

A Kinetic Model

Consistent with the weak effect of external TEA on the kinetics of slow inactivation of *Shaker* IR (Fig. 1), we

could not detect any effect on the voltage dependency of inactivation at near steady state (Fig. 2). On the other hand, *Shaker* IR T449S, the variant with enhanced C-type inactivation, was sensitive to external TEA, and accordingly, this pore blocker produced a significant shift along the voltage axis in the voltage dependence of steady-state inactivation (Fig. 4). Thus, we expected that the delay of the inactivation onset produced by internal TEA was accompanied by a shift along the voltage axis in the steady-state inactivation voltage dependency. It was somehow surprising that we could not detect any voltage shift after internal perfusion with 5 mM TEA (Fig. 8). Because inactivation kinetics is weakly voltage dependent (Olcese et al., 1997; Yang et al., 1997), these results suggest that slow inactivation occurs mostly after an important fraction of the gating charge has moved forward in the activation pathway. This suggestion is consistent with TEA having only a weak effect on the voltage dependence of the outward-gating charge movement elicited from a holding voltage of −90 mV (when most of the channels are closed), but preventing Q1 from changing to Q2 during inactivation (in the nomenclature of Olcese et al., 1997; see Fig. 11).

In the two-pulse protocols, external and internal TEA antagonize with the fast and the slow recovery phases, respectively (Fig. 10). These results suggest at least two separate slow inactivation pathways that within the time span of the experimental protocol essentially do not interconvert (see also, Klemic et al., 2001; Kurata et al., 2005). Thus, C-type inactivation recovers slowly, whereas the internal TEA-sensitive slow inactivation recuperates faster. Internal TEA slows down the closing of internally gated inactivation but does not affect its apparent rate of recovery (Fig. 10, inset), suggesting that this quaternary ammonium does not bind, or binds weakly, to the internally inactivated channels from the internal side.

The gating current experiments (Fig. 11) suggest two or more parallel energy pathways for the forward and backward movement of the gating charges; one corresponding to normal gating between closed states and the others to gating between slow-inactivated conformations. Thus, a minimal kinetic model to describe inactivation requires at least as many inactivated states as closed states (Olcese et al., 1997; Dougherty et al., 2008). In this case, such an allosteric type of model must have three parallel activation pathways, the normal, the C-inactivated, and the internally gated inactivation. Thus, we tested the allosteric kinetic model published by Klemic et al. (2001) for two coexisting inactivation pathways, the classical C-type inactivation and the U-type inactivation, here antagonized by internal TEA (Fig. 13A). In this model, *I* and *U* pathways are not directly interconnected as results shown in Fig. 10 suggest. Three additional states bound to internal TEA were attached: the open state (O_{TEA}), the last C-inactivated state (I_{5TEA}), and the last U-inactivated state (U_{5TEA}). This model resembles others used to describe closed-state inactivation in other Kv channels, a usually absorbing inactivated state visited from a pre-open closed conformation (Ayer and Sigworth, 1997; Kerschensteiner et al., 2003; Claydon et al., 2007; Dougherty et al., 2008). In this model, as the channel moves forward in the voltage activation pathway, it visits inactivated states increasingly faster by a constant allosteric factor and recovers increasingly slower by the same factor (see figure legend for details and Klemic et al., 2001).

Although the model was originally developed for different ionic conditions that could shift the voltage dependence of the activation (i.e., 5 mM K^+ and 4 mM Ca^{2+}), and considering that we did not alter the kinetic rate constants nor the allosteric factors, it is surprising how well it predicted several quantitative and qualitative aspects of the effects produced by 5 mM of internal TEA: (1) TEA increased the inactivation time constant by a factor of two as shown in Fig. 5. Such slowdown in the inactivation kinetics predicts a crossing in the time course of current decay at 0 mV (Fig. 13B). (2) TEA produced a shift of −2 mV in the voltage dependence of inactivation at near steady state (Fig. 13 C), below our detection limit, suggesting that the U-type inactivation state is mainly accessed from the C_3 and C_4, i.e., after a significant amount of charge has been mobilized to the active position in the normal activation pathway. (3) TEA reduces the amplitude of the fast recovery component without affecting its time constant (compare Fig. 13 D with Fig. 10 B). We could not, however, predict the clear increase in the fraction of Q1 in the gating currents elicited from holding voltage of 0 mV. We attribute this deficiency to the slow voltage-independent recovery rates k_i from the *I* states, where most of the channels reside in the presence of TEA, such that most of the charge returns through the *I* pathway. Manipulation of the rate constants or allosteric factors in the model could, in principle, provide a better description of the gating charge data. However, without additional experimental data designed to estimate such parameters, any modification to the model seems too arbitrary.

In the model shown in Fig. 13, the transit from the open state to the U-type inactivation at 0 mV is disfavored by the allosteric factor $g = 0.005$ or less (providing a destabilizing factor of 4×10^4 or higher), making state U_5 seldom visited (with at most <1% occupancy). With $g > 0.05$, the probability of U_{5TEA} is too high to give a reasonable account for the two-pulse data shown in Fig. 10, increasing, instead of decreasing, the size of the fast recovery component. On the other hand, values of $g <$ 0.005 or less provided a good qualitative description of the data (Fig. 13, B–D). Thus, the antagonism between slow inactivation and internal TEA results from the very low probability of existence of the states U_5-U_{5TEA} (with a combined probability of <0.01). For us, this condition is

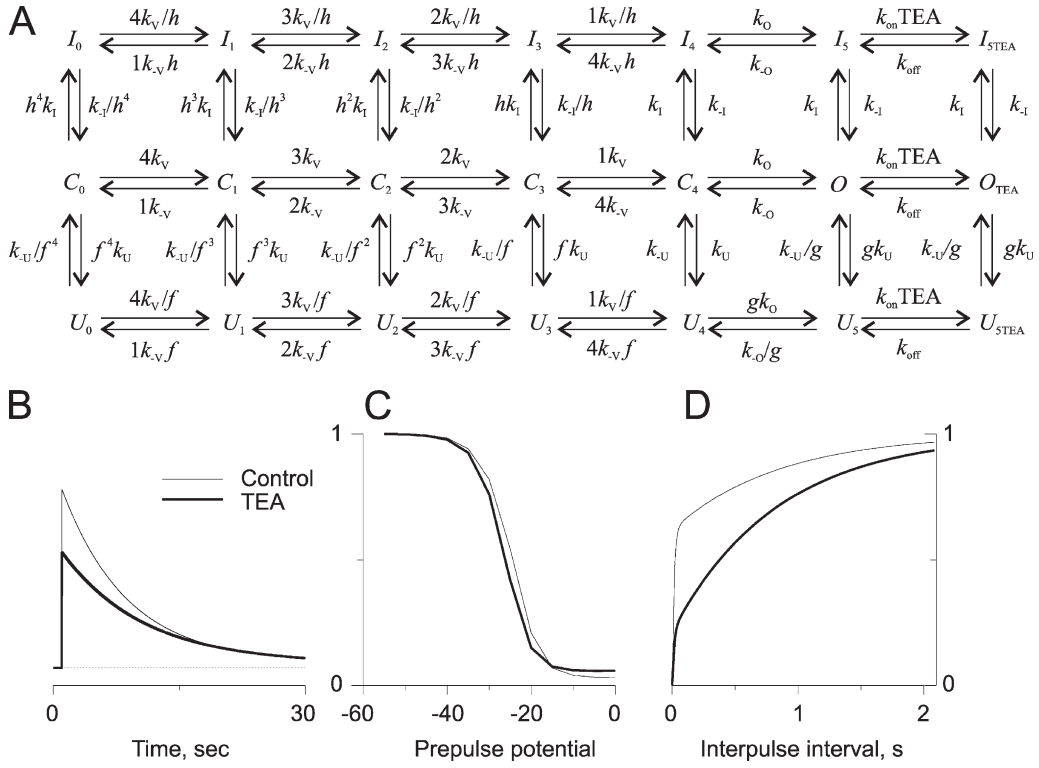

Figure 13. An allosteric kinetic scheme for slow inactivation of *Shaker* IR. (A) The kinetic scheme devised for U-type inactivation (Klemic et al., 2001) was modified to include blockade by internal TEA. The scheme contains three parallel activation pathways: *C*-inactivated, normal, and *U*-inactivated. Internal TEA binds with k_{on} = 2,400 $mM^{-1}s^{-1}$ and k_{off} = 2,400 s^{-1}. We changed the names of some variables such that: k_I = kp, k_I = k-p, k_U = ki, and k_U = k-i. All rate constants and allosteric factors are as in Klemic et al. (2001). (B) Simulated time course of macroscopic inactivation in response to a voltage step to 0 mV in the absence (thin trace) and presence of 0.6 mM TEA (thick trace). This TEA concentration is shown because we could not see crossing over of the traces for other TEA concentrations. (C) Normalized voltage dependence of the near equilibrium inactivation in the absence (thin trace) and presence of 5 mM internal TEA (thick trace). TEA produces a shift of −2 mV when fitted to a Boltzman distribution. (D) Normalized recovery from inactivation in the absence and presence of 5 mM TEA. The fast recovery time constant remained ∼15 ms under both experimental conditions, whereas the slow recovery retained a time constant of ∼840 ms. At 0-mV pulses, inactivation time constant changed from 7.7 s in the absence of TEA to 12.9 s with 5 mM TEA. The macroscopic inactivation rate decreased linearly with the fraction of unblocked current (see Fig. 7 D) with a slope of 0.065 s^{-1} and constant of 0.065 s^{-1}. On the other hand, the macroscopic deactivation rate constant at −110 mV decreased with a slope of 1.5 ms^{-1} as a function of the unblocked current, consistent with the magnitude and voltage dependence of k_O.

experimentally undistinguishable from a kinetic model in which internal TEA truly antagonizes U inactivation in a mutually exclusive fashion. Although similar in their numerical outcome, both modeling conditions, small allosteric factor *g* versus mutual exclusiveness, bring about dramatically different mechanistic implications. A small allosteric factor *g* implies that in the U-inactivated channels the internal TEA binding site is physically exposed. Whereas, classical mutually exclusive antagonism means that the binding site does not exist, or is not physically accessible, in the U-inactivated state. The addition of extra-infrequently visited states that provide an equally good qualitative description of the main features of our data can be justified because, for the model shown in Fig. 13, it delivers symmetry to the allosteric scheme. But it also introduces the allosteric factor *g*, a variable for which we do not envision a physical meaning.

But, not only parsimony mandates to shave away states U_5-U_{5TEA} from the scheme in Fig. 13. That the binding site for internal TEA does not exist, or is not physically accessible, in the U-inactivated channels is more appealing because it is consistent with current inactivation models proposed for other voltage-gated ion channels. As discussed below, functional, and possible physical, overlapping between the slow inactivation gate and the primary activation gate has been proposed for other members of the voltage-gated ion channel family (Sandtner et al., 2004; Shin et al., 2004; Dougherty et al., 2008).

Functional Overlapping between the Internal Slow Inactivation Gate and the Activation Gate

The existence of a single TEA binding site that would functionally interfere with activation and slow inactivation is consistent with a single putative site for the binding of TEA in the K channel pore in the open and closed conformations (Doyle et al., 1998; Jiang et al., 2002; Zhou et al., 2001b). This dual role of the TEA implies that both activation and deactivation gates either share

a significant extent of structural components, or are tightly functionally coupled. In agreement with this conclusion, there are a number of mutations in the second half of the inner helix that promote alterations in both slow inactivation and deactivation kinetics (see for example: Holmgren et al., 1997; D'Adamo et al., 1998; Sukhareva et al., 2003; Del Camino et al., 2005; Claydon et al., 2007; Klement et al., 2008). Additionally, in the *Shaker* homologue, Kv1.4, the conformational changes involving activation and slow inactivation displace a similar number of water molecules to/from the cytosolic face of the channel, implying similar volumetric changes in the internal vestibule (Jiang et al., 2003), revealing an intimate association between both gates.

In HCN and Kv4.2, other members of the voltage-gated K channel family, the primary activation gate recloses, or remains closed, during inactivation while its voltage sensors are in the active position (Shin et al., 2004; Dougherty et al., 2008). In these channels, inactivation is viewed as a voltage-desensitized state. Although internal TEA accessibility has not been tested in the inactivated state of these channels, interference by internal TEA, as observed here, is also expected to occur. U-type inactivation in *Shaker* K channels possibly occurs by reclosing of the activation gate. Such a mechanism seems to be widely present. For example, muscle sodium channel Nav1.4 also closes a cytosolic gate during ultraslow inactivation, a process interfered by intracellular applied lidocaine, presumably acting in a foot in the door fashion (Sandtner et al., 2004). Thus, it is not surprising that members of the same voltage-dependent ion channel protein family share a common repertoire of functional conformations. The balance of the time spend in each conformation, within a given physiological context, specifies the functional role of each ion channel. Thus, whether *Shaker*'s activation gate is closed or open during the internal TEA-sensitive slow inactivation remains to be tested.

We thank Ramón Latorre and John Ewer for insightful discussions and critical reading of the manuscript, and Victoria Prado for excellent technical help.

This work was funded by Programa Anillo de Ciencia y Tecnología award ACT (no. 46 to A. Neely and D. Naranjo), and PBCT PSD-20 (to P. Orio). During this work, V. González-Pérez and G. González-Gutiérrez were CONICYT doctoral fellows, and G. Rojas was a MECESUP UVA0603 doctoral fellow.

Edward N. Pugh Jr. served as editor.

Submitted: 3 June 2008
Accepted: 23 October 2008

REFERENCES

Armstrong, C.M. 1966. Time course of TEA+-induced anomalous rectification in squid giant axons. *J. Gen. Physiol.* 50:491–503.

Ayer, R.K. Jr., and F.J. Sigworth. 1997. Enhanced closed-state inactivation in a mutant *Shaker* K+ channel. *J. Membr. Biol.* 157:215–230.

Basso, C., P. Labarca, E. Stefani, O. Alvarez, and R. Latorre. 1998. Pore accessibility during C-type inactivation in Shaker K+ channels. *FEBS Lett.* 429:375–380.

Bernèche, S., and B. Roux. 2005. A gate in the selectivity filter of potassium channels. *Structure.* 13:591–600.

Bezanilla, F. 2000. The voltage sensor in voltage-dependent ion channels. *Physiol. Rev.* 80:555–592.

Baukrowitz, T., and G. Yellen. 1996. Use-dependent blockers and exit rate of the last ion from the multi-ion pore of a K+ channel. *Science.* 271:653–656.

Cha, A., and F. Bezanilla. 1997. Characterizing voltage-dependent conformational changes in the Shaker K+ channels with fluorescence. *Neuron.* 19:1127–1140.

Chen, J., V. Avdonin, M.A. Ciorba, S.H. Heinemann, and T. Hoshi. 2000. Acceleration of P/C-type inactivation in voltage-gated K+ channels by methionine oxidation. *Biophys. J.* 78:174–187.

Choi, K.L., R.W. Aldrich, and G. Yellen. 1991. Tetraethylammonium blockade distinguishes two inactivation mechanisms in voltage activated K+ channels. *Proc. Natl. Acad. Sci. USA.* 88:5092–5095.

Claydon, T.W., M. Vaid, S. Rezazadeh, S.J. Kehl, and D. Fedida. 2007. 4-aminopyridine prevents the conformational changes associated with P/C-type inactivation in shaker channels. *J. Pharmacol. Exp. Ther.* 320:162–172.

Cordero-Morales, J.F., V. Jogini, A. Lewis, V. Vásquez, D.M. Cortes, B. Roux, and E. Perozo. 2007. Molecular driving forces determining potassium channel slow inactivation. *Nat. Struct. Mol. Biol.* 14:1062–1069.

D'Adamo, M.C., Z. Liu, J.P. Adelman, J. Maylie, and M. Pessia. 1998. Episodic ataxia type-1 mutations in the hKv1.1 cytoplasmic pore region alter the gating properties of the channel. *EMBO J.* 17:1200–1207.

De Biasi, M., H.A. Hartmann, J.A. Drewe, M. Taglialatela, A.M. Brown, and G.E. Kirsch. 1993. Inactivation determined by a single site in K+ pores. *Pflugers Arch.* 422:354–363.

Del Camino, D., M. Kanevsky, and G. Yellen. 2005. Status of the intracellular gate in the activated-not-open state of shaker K+ channels. *J. Gen. Physiol.* 126:419–428.

Demo, S.D., and G. Yellen. 1991. The inactivation gate of the *Shaker* K+ channel behaves like an open-channel blocker. *Neuron.* 7:743–753.

Dougherty, K., J.A. De Santiago-Castillo, and M. Covarrubias. 2008. Gating charge immobilization in Kv4.2 channels: the basis of closed-state inactivation. *J. Gen. Physiol.* 131:257–273.

Doyle, D.A., J.M. Cabral, R.A. Pfuetzner, A.L. Kuo, J.M. Gulbis, S.L. Cohen, B.T. Chait, and R. Mackinnon. 1998. The structure of the potassium channel: molecular basis of K+ conduction and selectivity. *Science.* 280:69–77.

Ehrenstein, G., and D.L. Gilbert. 1966. Slow changes of potassium permeability in the squid giant axon. *Biophys. J.* 6:553–566.

García, E., M. Scanlon, and D. Naranjo. 1999. A marine snail neurotoxin shares with scorpion toxins a convergent mechanism of blockade on the pore of voltage-gated K channels. *J. Gen. Physiol.* 114:141–157.

Goldstein, S.A.N., D.J. Pheasant, and C. Miller. 1994. The charybdotoxin receptor of a shaker K^+ channel—peptide and channel residues mediating molecular recognition. *Neuron.* 12:1377–1388.

Hidalgo, P., and R. MacKinnon. 1995. Revealing the architecture of a K^+ channel pore through mutant cycles with a peptide inhibitor. *Science.* 268:307–310.

Hines, M.L., and N.T. Carnevale. 1997. The NEURON simulation environment. *Neural Comput.* 9:1179–1209.

Holmgren, M., P.L. Smith, and G. Yellen. 1997. Trapping of organic blockers by closing of voltage-dependent K+ channels: evidence for a trap door mechanism of activation gating. *J. Gen. Physiol.* 109:527–535.

Hoshi, T., W.N. Zagotta, and R.W. Aldrich. 1990. Biophysical and molecular mechanisms of Shaker potassium channel inactivation. *Science.* 250:533–538.

Hoshi, T., W.N. Zagotta, and R.W. Aldrich. 1991. Two types of inactivation in Shaker K+ channels: effects of alterations in the carboxy-terminal region. *Neuron.* 7:547–556.

Jerng, H.H., and W.F. Gilly. 2002. Inactivation and pharmacological properties of sqKv1A homotetramers in Xenopus oocytes cannot account for behavior of the squid "delayed rectifier" K+ conductance. *Biophys. J.* 82:3022–3036.

Jiang, X.J., G.C.L. Bett, X.Y. Li, V.E. Bondarenko, and R.L. Rasmusson. 2003. C-type inactivation involves a significant decrease in the intracellular aqueous pore volume of Kv1.4 K+ channels expressed in Xenopus oocytes. *J. Physiol.* 549:683–695.

Jiang, Y., A. Lee, J. Chen, M. Cadene, B.T. Chait, and R. MacKinnon. 2002. The open pore conformation of potassium channels. *Nature.* 417:523–526.

Kerschensteiner, D., F. Monje, and M. Stocker. 2003. Structural determinants of the regulation of the voltage-gated potassium channel Kv2.1 by the modulatory alpha-subunit Kv9.3. *J. Biol. Chem.* 278:18154–18161.

Klement, G., J. Nilsson, P. Arhem, and F. Elinder. 2008. A tyrosine substitution in the cavity wall of a k channel induces an inverted inactivation. *Biophys. J.* 94:3014–3022.

Klemic, K.G., G.E. Kirsch, and S.W. Jones. 2001. U-type inactivation of Kv3.1 and Shaker potassium channels. *Biophys. J.* 81:814–826.

Kurata, H.T., K.W. Doerksen, J.R. Eldstrom, S. Rezazadeh, and D. Fedida. 2005. Separation of P/C- and U-type inactivation pathways in Kv1.5 potassium channels. *J. Physiol.* 568:31–46.

Liu, Y., M.E. Jurman, and G. Yellen. 1996. Dynamic rearrangement of the outer mouth of a K+ channel during gating. *Neuron.* 16:859–867.

Loots, E., and E.Y. Isacoff. 1998. Protein rearrangements underlying slow inactivation of the Shaker K+ channel. *J. Gen. Physiol.* 112:377–389.

López-Barneo, J., T. Hoshi, S.H. Heinemann, and R.W. Aldrich. 1993. Effects of external cations and mutations in the pore region on C-type inactivation of Shaker potassium channels. *Receptors Channels.* 1:61–71.

Molina, A., P. Ortega-Sáenz, and J. López-Barneo. 1998. Pore mutations alter closing and opening kinetics in Shaker K+ channels. *J. Physiol.* 509:327–337.

Naranjo, D. 2002. Inhibition of single *Shaker* K channels by κ−conotoxin-PVIIA. *Biophys. J.* 82:3003–3011.

Olcese, R., R. Latorre, L. Toro, F. Bezanilla, and E. Stefani. 1997. Correlation between charge movement and ionic current during slow inactivation in Shaker K+ channels. *J. Gen. Physiol.* 110:579–589.

Oliva, C., V. González, and D. Naranjo. 2005. Slow inactivation in voltage gated potassium channels is insensitive to the binding of pore occluding peptide toxins. *Biophys. J.* 89:1009–1019.

Sandtner, W., J. Szendroedi, T. Zarrabi, E. Zebedin, K. Hilber, I. Glaaser, H.A. Fozzard, S.C. Dudley, and H. Todt. 2004. Lidocaine: a foot in the door of the inner vestibule prevents ultra-slow inactivation of a voltage-gated sodium channel. *Mol. Pharmacol.* 66:648–657.

Seoh, S.A., D. Sigg, D.M. Papazian, and F. Bezanilla. 1996. Voltage sensing residues in the S2 and S4 segments of the *Shaker* K+ channel. *Neuron.* 16:1159–1167.

Shin, K.S., C. Maertens, C. Proenza, B.S. Rothberg, and G. Yellen. 2004. Inactivation in HCN channels results from reclosure of the activation gate: desensitization to voltage. *Neuron.* 41:737–744.

Sukhareva, M., D.H. Hackos, and K.J. Swartz. 2003. Constitutive activation of the *Shaker* Kv channel. *J. Gen. Physiol.* 122:541–556.

Taglialatela, M., L. Toro, and E. Stefani. 1992. Novel voltage clamp to record small, fast currents from ion channels expressed in Xenopus oocytes. *Biophys. J.* 61:78–82.

Yang, Y.S., Y.Y. Yan, and F.J. Sigworth. 1997. How does the W434F mutation block current in Shaker potassium channels? *J. Gen. Physiol.* 109:779–789.

Yellen, G. 1998. The moving parts of voltage-gated ion channels. *Q. Rev. Biophys.* 31:239–295.

Yellen, G., D. Sodickson, T.Y. Chen, and M.E. Jurman. 1994. An engineered cysteine in the external mouth of a K1 channel allows inactivation to be modulated by metal-binding. *Biophys. J.* 66:1068–1075.

Zagotta, W.N., T. Hoshi, and R.W. Aldrich. 1990. Restoration of inactivation in mutants of Shaker potassium channels by a peptide derived from ShB. *Science.* 250:568–571.

Zhou, M., J.H. Morais-Cabral, S. Mann, and R. MacKinnon. 2001a. Potassium channel receptor site for the inactivation gate and quaternary amine inhibitors. *Nature.* 411:657–661.

Zhou, Y., J.H. Morais-Cabral, A. Kaufman, and R. MacKinnon. 2001b. Chemistry of ion coordination and hydration revealed by a K+ channel-Fab complex at 2.0 A resolution. *Nature.* 414:43–48.